Journal of Ceramic Processing Research. Vol. 21, No. 6, pp. 615~621 (2020)
(Received 30 August 2019, Received in revised form 26 December 2019, Accepted 21 January 2020)
https://doi.org/10.36410/jcpr.2020.21.6.615

J O U R N A L O F
Ceramic Processing Research

Synthesis and characterization of TiC powders by sol-gel method

Liang Gao[a,b], Yun Zhang[b,*], Xue Yang[b], YanBin He[b] and LiHua Song[b]
[a]*Heji Hospital Affiliated to Changzhi Medical College, Shanxi, 046012, China*
[b]*Department of pharmacy, Changzhi Medical College, Shanxi, 046012, China*

TiC powders were successfully synthesized by carbothermal reduction of Ti-O-C precursor in argon at 1,400 °C for 2 h. And the Ti-O-C precursor was formed by sol-gel method using titanium butyrate ($Ti(OC_4H_9)_4$), fructose ($C_6H_{12}O_6$), and acetyl acetone (*acac*). Here, *acac* was used as chemical modifier to control $Ti(OC_4H_9)_4$ hydrolysis to obtain stable sol. Furthermore, TG-DSC, XRD, FTIR, Raman, SEM, and EDS were employed to characterize the precursor and TiC powders. Moreover, *acac* as stabilizer was studied using FTIR when reacted with $Ti(OC_4H_9)_4$ formed stable six-member ring as a result of the existence of tautomer, prevent the nucleophilic attack of water, which reduced the hydrolysis rate of $Ti(OC_4H_9)_4$. Besides, the composition of TiC phase was further understood by the Raman spectra, and the results showed that the peaks at 403 cm^{-1}, 513 cm^{-1}, and 629 cm^{-1} were ascribed to the characteristic peaks of TiC. Finally, the photomicrograph revealed an equiaxed shape and the average grain size of TiC particles was ca. 1 um. The EDS indicated that the particles contain elements of Ti and carbon according to dot and line scan.

Keywords: Raman, sol-gel, FTIR, scan, TiC.

Introduction

Titanium carbide (TiC) has become an important nonoxide ceramic material as it possesses a number of desirable properties such as high melting temperature, high hardness, high modulus, high chemical stability, and good electrical conductivity [1-3]. Combined with high surface area and unique physical properties, TiC material has great potential for applications as leaning edge parts, rocket nozzle throat liners, hypersonic re-entry vehicles, jet engine components, and high-speed cutting tools [4-14]. However, the applications of TiC ceramic material have been limited as its strong covalent bonding contribute to properties of low self-diffusion coefficient and poor sintering ability [15, 16].

As known, the properties of powder have significant influence on the subsequent forming and sintering of ceramics, especially on the microstructure and mechanical properties of ceramics. In general, powders with high activity, high purity, and small particle size are conducive to the preparation of ceramic materials with uniform structure and high performance. Therefore, a synthesis method to meet the above requirements is needed. Until now, TiC powders can be prepared by high- temperature carbothermal reduction of a mixture of rutile (TiO_2) and carbon (C) according to reaction (1) [17]:

$$TiO_2(s) + 3C(s) = TiC(s) + 2CO(g)\uparrow \quad (1)$$

Carbothermal reduction was widely used to synthesize TiC due to a convenient process route, low cost of raw material, and capacity of production. However, such process usually required high temperature (1,700 ~ 2,100 °C) and a long production period. Besides this, several methods have been proposed to synthesize TiC powder, such as hydrogen plasma [18], mechanical alloying [19], microwave carbothermal reduction (CR) [20], petroleum coke salt bath [21], Mg thermal reduction [22], self-propagating high temperature synthesis (SHS) [23-25], and Chemical Vapor Deposition (CVD) [26]. However, such processes need an higher temperature or a long production period. Besides, the synthesized powders usually have a relatively coarse particle and a low purity. Comparing with traditional synthetic methods, the sol-gel chemical process with carbothermal reduction is a novel routine to synthesize metal carbides [27]. When prepared by a sol-gel technique, the polymeric precursor reactants are homogeneously distributed at a molecular level that reduces the kinetic barriers between the developed metal oxides and carbon particles created in pyrolysis of a metal alkoxide polymer precursor. Increased contact area of the nanoparticles results in carbothermal reduction of metal oxide and carbon at lower temperature and shorter time as compared to conventional methods of carbide synthesis. Moreover, the use of molecular precursors and the control of the process conditions allow preparation of homogeneous and pure multicomponent systems [27-31]. Actually, many ceramic powders have been synthesized by sol-

*Corresponding author:
Tel : +863558503489
Fax: +863558503489
E-mail: zhangyun0320@126.com

gel method. For example, Kwon et al. synthesized $K(Ta_{0.6}Nb_{0.4})O_3/SrTiO_3$ double layer thin films [32]. Muñiz-Serrato et al. prepared TiO_2 thin films by sol-gel method [33].

In the present study, a single phase of TiC powders was prepared by sol-gel method combining with carbothermal reduction process. Here, *acac* was used as chemical modifier to control $Ti(OC_4H_9)_4$ hydrolysis to obtain stable sol. Fructose was selected as carbon source because it can decompose to carbon and H_2O completely, so that the C/Ti molar ratio in the Ti-O-C precursor can be fixed precisely. Then, a metal alkoxide reaction system with *acac* was investigated by FTIR spectra. Besides, the Ti-O and Ti-B bonds were analyzed by FTIR and Raman spectra. And the elements of Ti and boron were investigated by energy dispersive spectrum (EDS).

Experimental

Titanium butyrate (TBOT, $Ti(OC_4H_9)_4$) and fructose ($C_6H_{12}O_6$) were utilized as starting materials in the present work. Acetylacetone (*acac*) was used as chelating agent and chemical modifier. Methyl alcohol (CH_3OH) and water (H_2O) were used as solvent. These materials were supplied by the Lanyi Reagents Co. Ltd., Beijing, China. The grade of all the above reagents was analytical.

In the present work, the TiC powders were synthesized by sol-gel method as shown in Fig. 1. In a typical synthesis, 3.0 g *acac* was dissolved in 25 mL of CH_3OH using a 80 mL beaker at 25 °C for 10 min on the magnetic stirrer. We refer to this solution as Solution 1. Then, 1.8 g of $C_6H_{12}O_6$ was dissolved in 5 mL of H_2O using a 80 mL beaker at 70 °C for 10 min in the water bath pot. We refer to this solution as Solution 2. Afterward, 6.8 g of $Ti(OC_4H_9)_4$ was dropwise added to the Solution 1. This was Solution 3. After that, the Solution 2 was slowly dripped into the Solution 3. Then, the sol was formed at 25 °C for 30 min. The resulting sol was heated with vigorous stirring to 80 °C and maintained for 2 h to form a wet gel. Finally, it was dried by freeze-drying under vacuum for 12 h followed by grinding process using an agate mortar and a pestle. In this way, a precursor was prepared. After that, the precursor was placed in alumina crucible using an alumina tube furnace in argon at 1,400 °C for 2 h. Then, the TiC powders were synthesized by carbothermal reduction according to the eq. (1).

The mass and heat flow of the samples were monitored by thermal analysis (TG-DSC, Beijing Hengjiu instrument Co. Ltd., Beijing, China). The crystallographic constitution was identified by means of an X-ray diffractometer (XRD) using graphite monochromatized CuK_a radiation (Rigaku, D/MAX 2200 PC). Crystallite size was estimated using the Debye-Scherrer equation,

$$D_{hkl} = 0.9\lambda / \beta_{hkl} \cos\theta \quad (2)$$

Where D_{hkl} is the crystallite size, λ is the wavelength of CuK_α radiation, β_{hkl} is the full-width at half maximum, and θ is the Bragg diffraction angle. The sol and precursor were characterized by FTIR in the range of 400 ~ 4,000 cm^{-1} using SHIMADZU 8400S apparatus. Raman spectra were measured with the spectrometer Aramis (Horiba Jobin Yvon) equipped with 532 nm laser. The morphology and element of the final products were characterized by SEM and EDS using a JEOL S4800 JAPAN microscope.

Results and Discussion

As known, metal alkoxides tend to react spontaneously with water and form precipitates resulting from successive hydrolysis and condensation reactions. In order to obtain a sol, $Ti(OC_4H_9)_4$ must be chemically modified by a complexing agent to decrease the alkoxide reactivity with water. In this work, *acac* was used as a chemical modifier. In order to reveal the transformation of chemical group and mechanism of reactions during the early stage of the synthesis process, the FTIR spectrums of *acac*, *Ti*(*acac*)$_2$ and precursor powders were presented

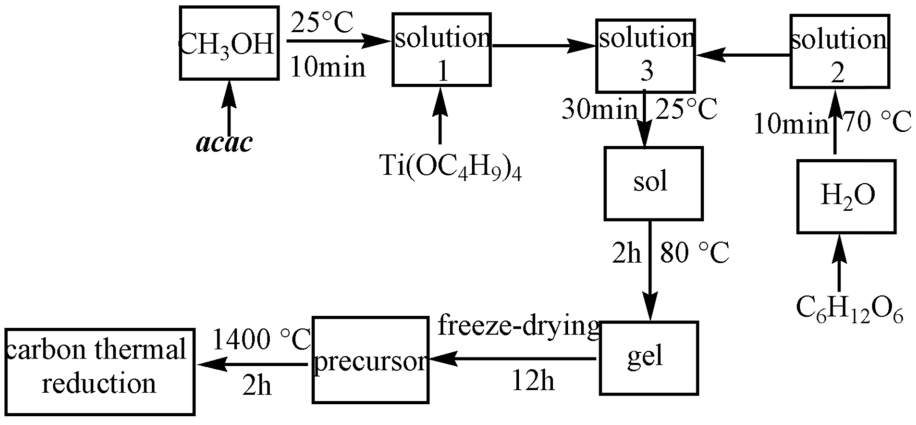

Fig. 1. Flow chart of synthesis of TiC powders.

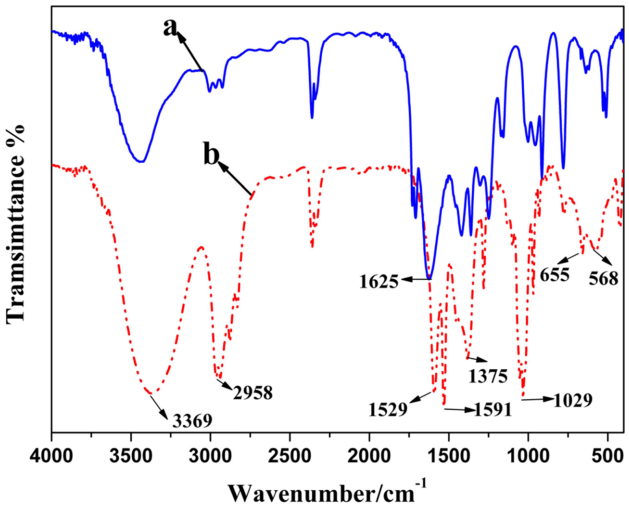

Fig. 2. FTIR spectra for starting material (*acac*) and material after being reacting with $Ti(OC_4H_9)_4$.

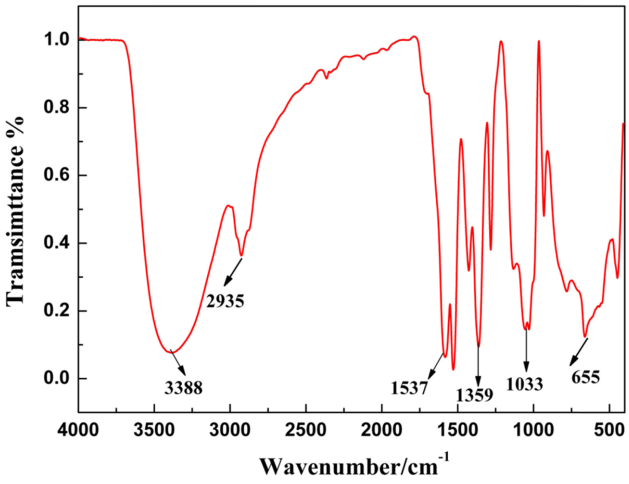

Fig. 3. FTIR spectra of TiC precusor.

in Fig. 2 and Fig. 3. Fig. 2(a) shows the FTIR of *acac*. It could be seen that the bond centred at 1,625 cm^{-1} was ascribed to the C=O double bond in *acac*. As can be seen from Fig. 2(b), the bands situated at 1591 and 1,529 cm^{-1} correspond, respectively, to the C=O and C=C stretching vibration of acetylacetone tautomers [34]. The C-H bending vibration of $RCH{=}CH_2$ was observed as a band close to 1,375 cm^{-1}. The band centered at 1,029 cm^{-1} corresponds to the C-O stretching vibration. Therefore, the keto-enol tautomeric formation occurs as the following equation [*see eq.* (3)]:

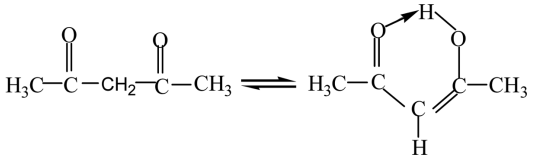

(3)

The electron withdrawing effect caused by the carbonyl makes the polarity of CH_2 increase and the α–H be a proton to derivate from the CH_2 bond easily [34]. The presence of n-BuOH, which was produced by the chelating reaction between alkoxide and acetylacetone, was corroborated by the bands located at 3369 and 655 cm^{-1} that were assigned to O-H stretching vibration and formation vibration in n-BuOH, respectively. As regards the broad band close to 568 cm^{-1}, it was deduced to correspond to the hexatomic ring vibration caused by the α–H of acetylacetone substituting for the BuO– band. Therefore, the chelation reaction between the $Ti(C_4H_9O)_4$ and acetylacetone is deduced to take place according to the following equation [34]:

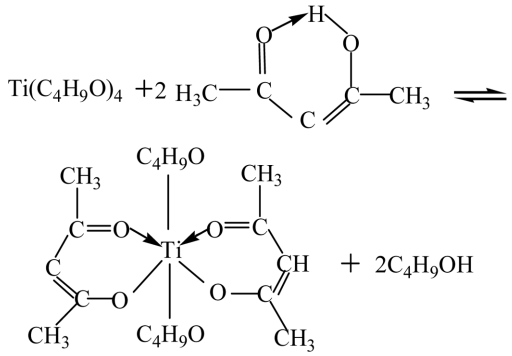

(4)

As a chelating agent, the acetylacetone not only substitutes the alkoxy group of the double alkoxide to enhance the steric effects, but also forms steady hexatomic rings, which embarrasses the nucleophilic attack of water molecule to the alkoxide and slows down the hydrolysis effectively. According to different needs, diverse kinds and amount of chelating agent could be added to control the structure of gel and achieve the intention of designing and tailoring molecules. Then, the processes of hydrolysis and concentration were taken place in the following equations [*see eq.* (5) - (8)].

$$\equiv Ti\text{-}OC_4H_9 + H_2O \rightleftharpoons \equiv Ti\text{-}OH + C_4H_9OH \quad (5)$$

$$\equiv Ti\text{ -acac} + H_2O \rightleftharpoons \equiv Ti\text{ -}OH + C_5H_8O_2 \quad (6)$$

$$\equiv Ti\text{-}OC_4H_9 + HO\text{-}Ti\equiv \rightleftharpoons \equiv Ti\text{-}O\text{-}Ti\equiv + C_4H_9OH \quad (7)$$

$$\equiv Ti\text{-}OH + HO\text{-}Ti\equiv \rightleftharpoons \equiv Ti\text{-}O\text{-}Ti\equiv + H_2O \quad (8)$$

Fig. 3 shows the FTIR of precusor powder. Acorrding to literature[35], the peak of 655 cm^{-1} was attributed to stretching vibration of Ti-O bond. And the peaks of 1,033 cm^{-1}, 1,359 cm^{-1}, 1,537 cm^{-1}, 2,935 cm^{-1} and 3,388 cm^{-1} were attributed to stretching vibrations of $–CH_2$, $–CH_3$, and O-H bonds, respectively. The results of FTIR explained what happened in the preparing process of sol and precursor.

TG-DSC analysis in argon was conducted to understand the thermal behavior and reactions of precursor during the heat treatment from room temperature to 900 °C. The complementary information obtained allows differentiation between endothermic and exothermic events which have no associated weight loss (*e.g.* melting and crystallization)

and those which involve a weight loss (*e.g.* degradation). TG analysis showed that a considerable weight loss occurred in a temperature range of 92 ~ 590 °C for the precursor as shown in Fig. 4. The whole process could be divided into two stages according to TG curve. The first stage of weight loss was mainly caused by the evaporation of water less than 200 °C. The second stage was completely caused by the transformation of $C_6H_{12}O_6$ to amorphous carbon and H_2O from 200 °C to 590 °C ($C_6H_{12}O_6$ = 6C + 6H_2O). Alternatively, DSC curve in Fig. 4 revealed that one endothermic peaks and a broad exothermic peak during these stages. It could be explained that the former was mainly attributed to the evaporation of the bonded water and the latter could be correlated with the transformation of $C_6H_{12}O_6$, remaining organic compounds and crystallization of TiO_2.

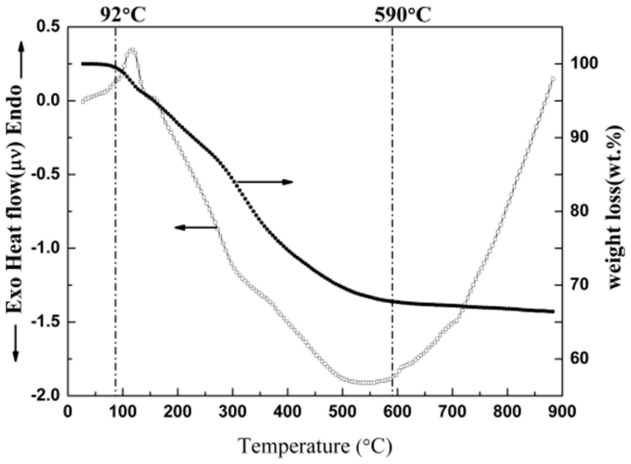

Fig. 4. TG-DSC of TiC precursor from room temperature to 900 °C in argon.

Moreover, the weight loss was slow and the DSC curve was approximately straight as well from 600 °C to 900 °C. It could be revealed that there was only the change of crystallinity and crystal transformation of TiO_2 during this stage, and scarcely any other reactions. That is to say, the main weight loss of precursor was mainly caused by the evaporation of water and the decomposition of $C_6H_{12}O_6$ during the process of heating.

Based on the above results of the thermal analysis, the precursor was firstly heated to 600 °C in order to completely transform $C_6H_{12}O_6$, then to 1,100 °C at 3 °C/min and maintained at this temperature for 2 h in argon using an alumina tube furnace. Afterwards, the precursor powder was continued to heat from 1,100 °C to 1,400 °C at a heating rate of 2 °C/min and kept at this temperature for 2 h. Then, the sample was cooled to room temperature at a cooling rate of 5 °C/min. Fig. 5 shows XRD patterns of the TiC precursor powders calcined at different temperatures. Clearly, the precursor was in a typical amorphous state without any peak in its XRD pattern [see Fig. 5(a)]. Fig. 5(b) shows the XRD pattern of the precursor heated at 1,400 °C for 2 h in argon, the peaks of TiC have been found at 2θ = 41.7°, 35.9°, 60.4°, 72.3°, and 76.1° respectively. That is to say, a single phase of TiC evolves by heating at 1,400 °C, for 2 h. And the reaction temperature of synthesizing TiC powders was much lower than other traditional method, which could be attributed to the homogeneous mixing and enormous contact area of reactants in the precursor. In this work, the experimental conditions were limited, so the temperature was only

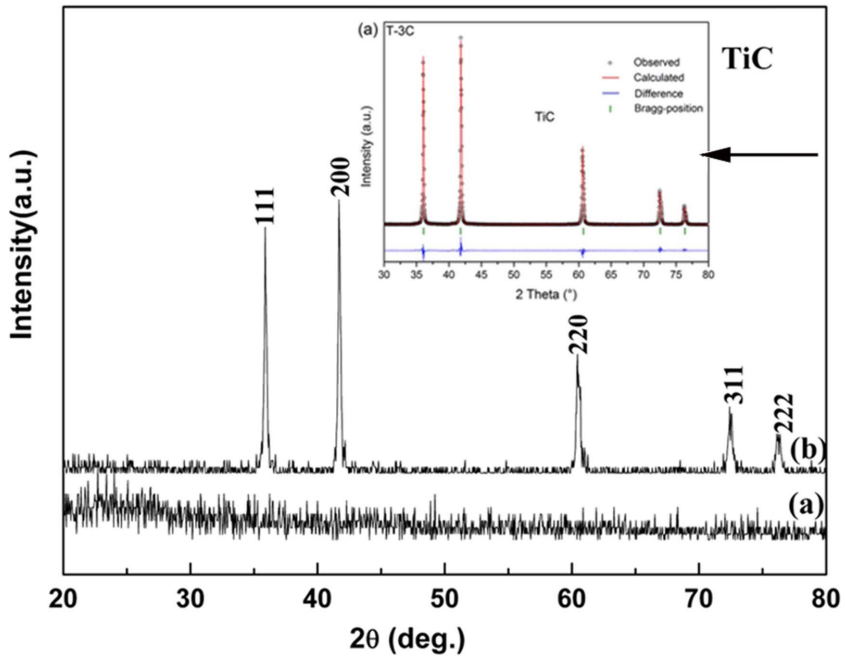

Fig. 5. XRD of patterns of (a) precursor, and the precursor reduced carbothermally at (b) 1,400 °C.

raised 1,400 °C. A further study was conducted to evaluate the average particle / grain size based on the Debye-Scherrer equation. The result reveals that it was about 1 um.

Raman spectroscopy involves the spectral analysis of the light produced by the inelastic scattering of monochromatic light by molecules or crystal lattices. This information can then be used to determine details of the structure of the molecule or crystal lattice. As reported in literature, stoichiometric TiC is Raman inactive due to the high inversion symmetry present in the O_h point group of the crystal structure of TiC, and the screening effect of the valence electron present in most metallic bonds [36-38]. However, non-stoichiometric TiC_{1-x} has been reported to be Raman-active, probably due to the presence of carbon vacancies, deformation defects and lattice imperfections contained in the off-stoichiometric TiC_{1-x} structure. A Raman spectroscopic signal for off- stoichiometric TiC_{1-x} has been reported by Lohse et al. [39], Klein et al. [36], Amer et al. [37], Huong et al. [40], Oláh et al. [41], and Pellegrino et al. [42]. Essentially, Klein et al. reported normal vibrations of off-stoichiometric TiC_{1-x} bonds that corresponds to Raman-active modes [*see eq.*(9)][36].

$$\Gamma = A_{1g}+E_g+T_{2g} \quad (9)$$

Fig. 6 shows the Raman spectra of the synthesized TiC powder which give further insight into the depth of the TiC phase formation. Obviously, there were not any peaks in the Raman spectra in Fig. 6(a). As can be seen from Fig. 6(b), Raman spectra obtained for the synthesized TiC powder were observed to display five characteristic peaks. Two of the peaks were broad and were located at 1,384 and 1,573 cm^{-1}, assigned respectively to A_{1g} and E_{2g} Raman-active modes of carbon while the other three peaks that were located at 403, 513, and 629 cm^{-1} were reportedly associated to signal of Ti-C bond vibrations of off-stoichiometric TiC_{1-x} [39, 37]. According to Klein et al. [36], these three peaks were assigned to Raman-active modes. The A_{1g} and E_g peaks, typically located in the optical phonons region were vibrational bond motion due to the carbon atom while the T_{2g} peak located within the acoustic region is associated with the titanium motion [36]. This implies that the vibrational bond contribution due to carbon atoms present in the off-stoichiometric TiC_{1-x} is probably stronger than motion that comes from the titanium bonded atoms. That is to say, in addition to TiC, there was a small amount of carbon in the powder.

In general, the morphology of particles is a comprehensive reflection of the synthesis reactions and processes. Energy dispersive spectrum (EDS) reveals the distribution of elements; these distributions can be displayed as either dot maps or line profiles to distinguish particles with different chemical compositions. Fig. 7 shows a SEM image of TiC powders carbothermally reduced at 1,400 °C for 2 h. The SEM image revealed TiC particles with equiaxed shape and the particle size was uniform, around 1 um in diameter. The EDS indicated that the particle contains Ti and carbon (arrowhead). Additionally, the EDS of one particle was not completely proven the whole TiC powders, so it was necessary to do the EDS line scan for particles (arrowhead) (see Fig 8(a)). The straight line in Fig. 8(b) was a reference line for the

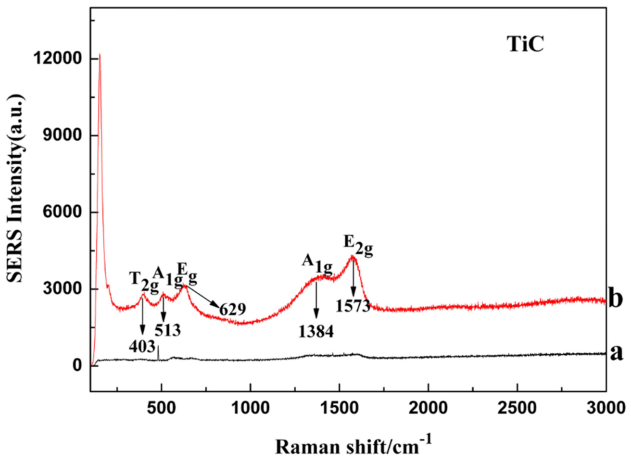

Fig. 6. Raman spectra of (a) precursor; (b) TiC powders.

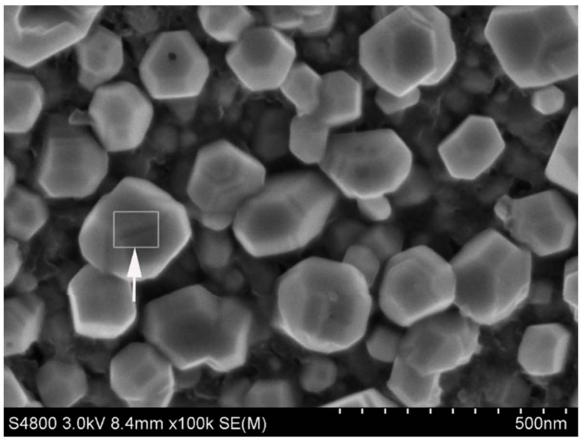

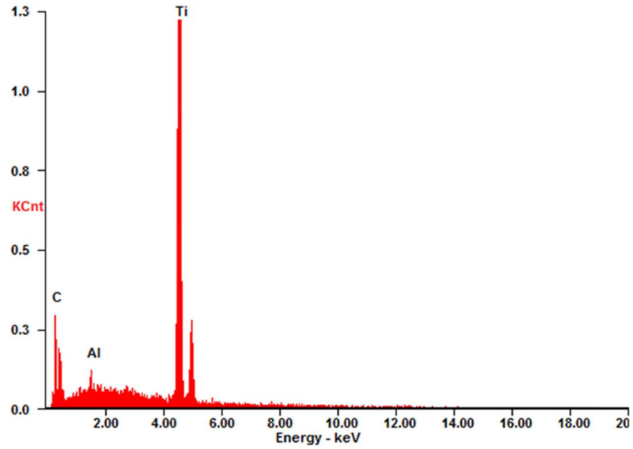

Fig. 7. SEM image of TiC powders along with the EDS pattern.

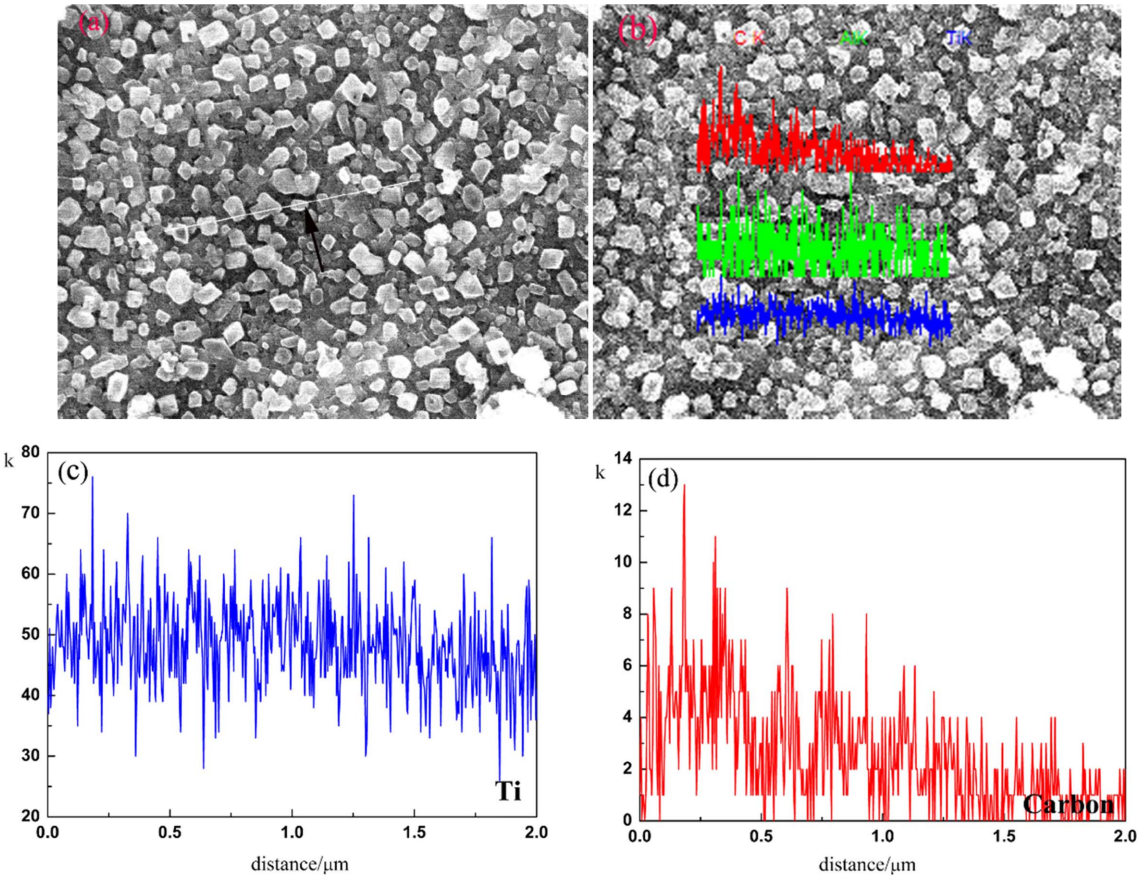

Fig. 8. SEM image TiC powders (a, b), and the EDS spectra for elements Ti (c) and carbon (d).

EDS line scan; the signal profiles of line scans for Ti and carbon following this reference line were also shown. Figs. 8(c) and (d) show the total recorded EDS line scans for Ti and carbon, respectively. The EDS profiles of line scans shown in Fig. 8(b) were consistent with the scans in Figs. 8(c) and (d). When scanning along the reference line, the synchronized alternation of Ti and carbon signals were clearly seen in Figs. 8(c) and (d). That is to say, the changes in Ti and carbon contents with distance across the particles were similar and just as for the line scans, Ti and carbon showed similar behavior.

Conclusions

TiC powders were synthesized by sol-gel method using $Ti(OC_4H_9)_4$ and $C_6H_{12}O_6$ as starting materials. It was notable that the monophasic TiC could be obtained at 1,400 °C for 2 h in argon. Moreover, *acac* as stabilizer reacted with $Ti(OC_4H_9)_4$ formed stable six-member ring due to the existence of tautomer, prevent the nucleophilic attack of water, which reduced the hydrolysis rate of $Ti(OC_4H_9)_4$. Besides, the formation of TiC phase was characterized not only by XRD but also by Raman and the results showed that the peaks at 403 cm^{-1}, 513 cm^{-1}, and 629 cm^{-1} were ascribed to the characteristic peaks of TiC in Raman spectra. Finally, the SEM shows TiC powders with equiaxed shape and the average grain size of TiC particles was ca. 1 um. And EDS indicated that the particles contain elements of Ti and carbon according to dot and line scan.

Acknowledgments

This work was supported by Doctoral Scientific Research Foundation of Changzhi Medical College (BS201915), Applied Basic Research Program of Shanxi Province (201701D221046), and Innovation Team Project of Changzhi Medical College (CX201904).

References

1. 1.M.B. Rahaei, R.Y. Rad, A. Kazmzadeh, and T. Ebadzadeh, Powder Tech. 217 (2012) 369-376.
2. S.B. Li, W.H. Xiang, H.X. Zhai, and Y. Zhou, Powder Tech. 185 (2008) 49-53.
3. C. Benoit, H. Ellen, K. Nikhil, V. Dominique, and D. Sylvain, Powder Tech. 157[1-3] (2005) 92-99.
4. S. Li, K. Kondoh, H. Imai, B. Chen, L. Jia, J. Umeda, and Y. Fu, Mater. Des. 95 (2016) 127-132.
5. L. Cheng, Z. Xie, and G. Liu, J. Eur. Ceram. Soc. 33[15-16] (2013) 2971-2977.
6. C. Magnus, T. Kwamman, and W.M. Rainforth, Wear 422-423 (2019) 54-67.
7. J. Zhang, L. Wang, W. Jiang, and L. Chen, Mater. Sci. Eng.

A 487[1-2] (2008) 137-143.
8. B. Zou, W. Ji, C. Huang, J. Wang, S. Li, and K. Xu, J. Alloy. Comp. 585 (2014) 192-202.
9. S. Liu and D. Liu, Int. J. Refract. Metals Hard Mater. 82 (2019) 273-278,
10. M. Sribalaji, B. Mukherjee, S.R. Bakshi, P. Arunkumar, K. Suresh Babu, and A.K. Keshri, Compos. B Eng. 123 (2017) 227-240.
11. J.X. Xue, J.X. Liu, G.J. Zhang, H. Bin Zhang, T. Liu, X.S. Zhou, and S.M. Peng, Scr. Mater. 114 (2016) 5-8.
12. X. Yue, Z. Cai, X. Lü, J. Wang, and H. Ru, Mater. Sci. Eng. A 668 (2016) 208-214.
13. Z. Shi, W. Shao, T. Hu, C. Zhao, X. Xing, Y. Zhou, and Q. Yang, J. Alloy. Comp. 805 (2019) 1052-1059.
14. L. Cheng, Z. Xie, and G. Liu, Ceram. Int. 39[5] (2013) 5077-5082.
15. X. Chen, J. L. Fan, and Q. Lu, J. Solid State Chem. 262 (2018) 44-52.
16. S. Mohapatra, D.K. Mishra, and S.K. Singh, Powder Tech. 237 (2013) 41-45.
17. Y.C. Woo, H.J. Kang, and D.J. Kim, J. Eur. Ceram. Soc. 27[2-3] (2007) 719-722.
18. L. Tong and R.G. Reddy, Scr. Mater. 52[12] (2005) 1253-1258.
19. M. Razavi, M.R. Rahimipour, and A.H. Rajabi-Zamani, J. Alloys Compd. 436[1-2] (2007) 142-145.
20. X.L. Hu, Y. Liu, W.N. Zhang, K. Chen, H. Yin, L.K. Zeng, Z.X. Chen, and Z.L. Zhao, China Patent 01129991.6. (2003)
21. L.S. Cui, J.L. Zhao, X.L. Cui, Y.J. Zheng, and W.F. Gao, China Patent 02159005.2. (2006)
22. D.W. Lee and B.K. Kim, Scr. Mater. 48[11] (2003) 1513-1518.
23. L.L. Ye and M.X. Quan, Nanostruct. Mater. 5 (2001) 103-105.
24. B. Ghosh and S.K. Pradhan, Mater. Chem. Phys. 120[2-3] (2010) 537-545.
25. M. Razavi, M. R. Rahimipour, and R. Kaboli, J. Alloy Compd. 460[1-2] (2008) 694-698.
26. R. Alexandrescu, E. Borsella, S. Botti, M.C. Cesile, S. Martelli, R. Giorgi, S. Turtu, and G. Zappa, J. Mater. Sci. 32 (1997) 5629-5635.
27. M.D. Sacks, C. Wang, Z. Yang, and A. Jain, J. Mater. Sci. 39 (2004) 6057-6066.
28. C.R. Rambo, J. Cao, O. Rusina, and H. Sieber, Carbon 43[6] (2005) 1174-1183.
29. H. Zhang, F. Li, Q. Jia, and G. Ye, J. Sol-Gel Sci. Technol. 46(2008) 217-222.
30. M. Umalas, V. Reedo, A. Lohmus, I. Hussainova, and K. Juhani, Key Eng. Mater. 527 (2012) 62-67.
31. C. Giordano and M. Antonietti, Nano Today 6[4] (2011) 366-380.
32. M.S. Kwon, S.G. Lee, and K.M. Kim, J. Ceram. Process. Res. 19[4] (2018) 316-320.
33. O.M. Serrato and J.S. Rodríguez, J. Ceram. Process. Res. 19(4) (2018) 306-310.
34. W. Liu, J.L. Yang, H. Xu, Y.Z. Wang, S.L. Hu, and C.Y. Xue, Adv. Powder Tech. 24[1] (2013) 436-440.
35. X. Chen, J.L. Fan, and Q. Lu, J. Solid State Chem. 262 (2018) 44-52.
36. M.V. Klein, J.A. Holy, and W.S. Williams, Phys. Rev. B 17 (1978) 1546-1556.
37. M. Amer and M.W. Barsoum, J. Appl. Phys. 84 (1998) 5817-5824.
38. J.R. Ferraro, K. Nakamoto, and C.W. Brownand, in "Introductory Raman Spectroscopy" (Academic Press, 2003) p.406-421.
39. B.H. Lohse, A. Calka, and D. Wexler, J Alloys Compd 434-435 (2007) 405-409.
40. P.V. Huong, A.L. Verma, J.P. Chaminade, L. Nganga, and J.C. Frison, Mater. Sci. Eng. B 5[2] (1990) 255-260.
41. N. Oláh, M. Veres, A. Sulyok, M. Menyhárd, J. Gubicza, and K. Balázsi, J. Eur. Ceram. Soc. 34[1-4] (2014) 3421-3425
42. S. Pellegrino, L. Thomé, A. Debelle, S. Miro, and P. Trocellier, Atoms. 327 (2014) 103-107.